

# *AKARI* Detection of the Infrared-Bright Supernova Remnant B0104–72.3 in the Small Magellanic Cloud

Bon-Chul KOO<sup>1</sup> Ho-Gyu LEE<sup>1</sup> Dae-Sik MOON<sup>2</sup> Jae-Joon LEE<sup>1</sup> Ji Yeon SEOK<sup>1</sup> Hyung Mok LEE<sup>1</sup> Seung Soo HONG<sup>1</sup> Myung Gyoon LEE<sup>1</sup> Hidehiro KANEDA<sup>3</sup> Yoshifusa ITA<sup>3</sup> Woong-Seob JEONG<sup>3</sup> Takashi ONAKA<sup>4</sup> Itsuki SAKON<sup>4</sup> Takao NAKAGAWA<sup>3</sup> Hiroshi MURAKAMI<sup>3</sup>

<sup>1</sup>*Department of Physics and Astronomy, Seoul National University, Seoul 151-742, KOREA*  
*koo@astrohi.snu.ac.kr; hglee@astro.snu.ac.kr; jjlee@astro.snu.ac.kr; jyseok@astro.snu.ac.kr;*  
*hmlee@astro.snu.ac.kr; sshong@astro.snu.ac.kr; mglee@astro.snu.ac.kr*

<sup>2</sup>*Department of Astronomy and Astrophysics, University of Toronto, Toronto, ON M5S 3H4, CANADA*  
*moon@astro.utoronto.ca*

<sup>3</sup>*Institute of Space and Astronautical Science, Japan Aerospace Exploration Agency, Sagami-hara, Kanagawa 229-8510, JAPAN*  
*kaneda@ir.isas.jaxa.jp; yita@ir.isas.jaxa.jp; jeongws@ir.isas.jaxa.jp; nakagawa@ir.isas.jaxa.jp;*  
*hmurakam@ir.isas.jaxa.jp*

<sup>4</sup>*Department of Astronomy, Graduate School of Science, University of Tokyo, Bunkyo-ku, Tokyo 113-0003, JAPAN*  
*onaka@astron.s.u-tokyo.ac.jp; isakon@maitta.astron.s.u-tokyo.ac.jp*

(Received 2007 February 0; accepted 2007 March 0)

## Abstract

We present a serendipitous detection of the infrared-bright supernova remnant (SNR) B0104–72.3 in the Small Magellanic Cloud by the Infrared Camera (IRC) onboard *AKARI*. An elongated, partially complete shell is detected in all four observed IRC bands covering 2.6–15  $\mu\text{m}$ . The infrared shell surrounds radio, optical, and X-ray emission associated with the SNR and is probably a radiative SNR shell. This is the *first* detection of a SNR shell in this near/mid-infrared waveband in the Small Magellanic Cloud. The IRC color indicates that the infrared emission might be from shocked H<sub>2</sub> molecules with some possible contributions from ionic lines. We conclude that B0104–72.3 is a middle-aged SNR interacting with molecular clouds, similar to the Galactic SNR IC 443. Our results highlight the potential of *AKARI* IRC observations in studying SNRs, especially for diagnosing SNR shocks.

**Key words:** ISM: individual (B0104–72.3) – Magellanic Clouds – supernova remnants

## 1. Introduction

The Small Magellanic Cloud (SMC) has about twenty known SNRs. They have been identified and studied mostly in radio, X-ray, and optical bands (Mathewson et al. 1984; van der Heyden et al. 2004; Filipović et al. 2005 and references therein). Infrared studies are very limited in spite of their advantages in understanding the interstellar medium of this nearby, metal-poor irregular galaxy as well as in understanding the nature of SNRs.

In this paper, we report the detection of the SNR B0104–72.3 (J010619–720527; IKT 25; hereafter B0104–72.3) in the SMC in the 2.6–15  $\mu\text{m}$  range by the Infrared Camera (IRC) onboard *AKARI*. This is the *first* SNR detected in this IR band in the SMC. The only other SNR detected in mid-infrared waveband in the SMC is the radio/X-ray bright SNR B0102.2–72.19, which was observed by Stanimirović et al. (2005) using the *Spitzer Space Telescope* and detected only at 24  $\mu\text{m}$ . B0104–72.3 is the faintest radio SNR in the SMC, located in the northwestern area of the “wing” close to the “bar”. It is small (100” or 29 pc at the distance of 60 kpc), and its radio structure is not well resolved (Mathewson et al. 1984; Filipović et al. 2005). The faintness together with its relatively small spatial extent led Mathewson et al. (1984) to suggest that it is possibly a Balmer-dominated Type Ia SNR. On the other hand, the remnant has a flat radio spectrum with a spectral index  $\alpha = 0.19 \pm 0.28$  ( $S_\nu \propto \nu^\alpha$ ; Filipović et al. 2005), which suggests a possibility of Crab-like SNR or ‘plerion’. The remnant has been studied in X-rays using *ROSAT* and *XMM*. Hughes et al. (1994) showed that the X-ray emission is composed of a diffuse emission extending along the north-south direction and a point-like source at the southern end. They tentatively identified the point-like source as a Be/X-ray binary system and proposed a core-collapse SN origin for the remnant. van der Heyden et al. (2004) obtained an X-ray spectrum of the remnant using the *XMM-Newton* observatory and showed that the Fe abundance is enhanced with respect to the mean O, Ne and Mg abundance values. They concluded that the X-ray emission is possibly from ejecta remains of Type Ia. In summary, the radio and X-ray observations do not yield a coherent picture on the nature of the remnant. We show that B0104–72.3 has a well defined IR shell surrounding the radio, optical, and X-ray emissions and that B0104–72.3 is probably interacting with molecular clouds. We discuss the nature of the SNR based on *AKARI* observations.

## 2. Serendipitous Detection

B0104–72.3 was detected serendipitously during the pointed observation of the oxygen-rich SNR B0103–72.6 (DEM S125; Park et al. 2003) in the SMC using the *AKARI* IRC on November 8, 2006. The IRC is equipped with three waveband channels with  $10' \times 10'$  field-of-view (FOV), which operate simultaneously at any exposure time (Onaka et al. 2007). Among them the NIR and MIR-S channels share the same FOV, while the MIR-L channel has FOV 25' away from them. B0104–72.3 happened to be in the NIR/MIR-S FOV when B0103–72.6 was

centered at the MIR-L FOV. We used the two-filter mode (IRC02), which gave two band images at each channel: N3 and N4 in NIR, and S7 and S11 in MIR-S. N3, N4, S7, and S11 images have isophotal wavelengths of 3.19, 4.33, 7.12 and 10.45  $\mu\text{m}$  with effective bandwidths of 0.87, 1.53, 1.75 and 4.12  $\mu\text{m}$ , respectively. The pixel sizes of the NIR and MIR-S channels are 1.''46 and 2.''34, respectively. The angular resolutions are 4.''0, 4.''2, 5.''1, and 4.''8 in N3, N4, S7, and S11, respectively (Onaka et al. 2007). The total on-source integration times were 178 s for NIR and 196 s for MIR-S. The basic calibration and data handling including dark subtraction, linearity fitting, distortion correction, flat fielding, and image combining were processed using the standard IRC Imaging Data Reduction Pipeline version 070104 (Ita & Pearson 2007). We, however, used our own flat images derived from the North Ecliptic Pole data around our observing date for the MIR-S, because the IRC MIR-S flats have noticeable “dark pattern” and, if we use the provided superflats, it leaves an artifact even after the flat-fielding (see IRC Data User’s Manual). The astrometric solutions were obtained by matching with the coordinates of 2MASS stars in the field using the Pipeline process *putwcs*. The resulting positional uncertainty ( $1\sigma$ ) is  $\leq 0.''4$  for N3, N4, S7, and  $1''$  for S11.

Fig. 1 shows *AKARI* images of B0104–72.3. A partially-complete shell structure is apparent in all four bands. The shell is elongated along the northeast-southwest direction and has a bright, well-defined circular northeastern portion (hereafter the IR-NE shell). The brightness of the IR-NE shell is not uniform, and there is a prominent bright spot at the southern end which is marked by a white cross. The maximum, background-subtracted brightness of the spot is  $\sim 0.11, 0.17, 0.41,$  and  $0.42 \text{ MJy sr}^{-1}$  in N3, N4, S7, and S11, respectively. The rest part of the shell is mostly missing, but, to the southwest, a small segment of the shell (the IR-SW shell), which has a curvature opposite to the IR-NE shell, is visible. Some faint, filamentary emission is also visible between the two shell parts. These IR-NE and IR-SW shells surround the radio emission neatly (see next section), so that they are likely to be parts of the SNR shell. The extent of the SNR determined from Fig. 1 is  $100'' \times 65''$  (or  $29 \text{ pc} \times 19 \text{ pc}$ ).

### 3. Comparison with Other Waveband Images

Fig. 2 is our three-color image representing the N4 (B), S7 (G), and S11 (R) emission of B0104–72.3. The white contours represent the 843 MHz radio map (FWHM= $43''$ ) from the Molonglo Observatory Synthesis Telescope (Mathewson et al. 1984). The radio emission is elongated along the northeast-southwest direction and almost perfectly fits into the IR shell. It has the maximum inside the IR-NE shell and an extended ‘plateau’ to southwest, which is confined to a relatively narrow region. The 2.37 GHz map (FWHM= $40''$ ) of Filipović et al. (2005) obtained by using the Australian Telescope Compact Array shows essentially the same radio morphology. It is possible that the remnant has a shell structure in the radio too but is smeared because of the poor resolutions of these interferometric observations. We have simulated how the remnant would appear with a large beam if the radio brightness is

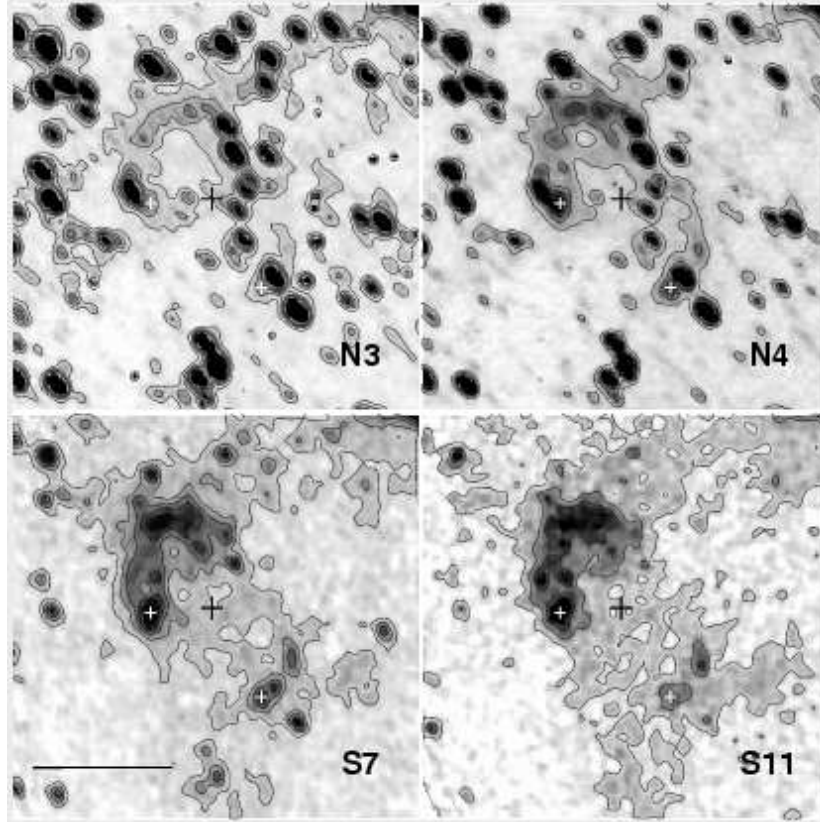


**Fig. 1.** *AKARI* images of the SNR B0104–72.3 in N3, N4, S7, and S11 bands. Contour levels are linearly spaced starting at 0.18, 0.30, 3.90, and 16.4 MJy sr<sup>-1</sup> with steps of 0.04, 0.04, 0.06, and 0.1 MJy sr<sup>-1</sup> in N3, N4, S7, and S11 images, respectively. The N3 and N4 images show trails of pixels with enhanced brightness, which is a detector artifact called multiplexer bleed, or “muxbleed” (IRC Data User’s Manual). The black cross marks the geometrical center of the shell at (01<sup>h</sup> 06<sup>m</sup> 18.<sup>s</sup>3, –72° 05′ 37”). The white crosses mark the peak positions in the S7 band. The scale bar in the S7 image represents an angular size of 1′. North is up and east is to the left.

proportional to that of the IR shell. We convolved the S7 image, where the shell is most prominent, with a Gaussian beam of FWHM=43”. The simulated map also shows a centrally brightened remnant, but its peak occurs close to the IR-NE shell,  $\sim 15''$  north to the peak of the 843 MHz emission. Another difference between the simulated and the observed radio maps is that, in the former, there is a separate peak at the position of the IR-SW shell while, in the latter, the intensity decreases smoothly toward the southwest. The above comparison leads us to conclude that the radio brightness distribution should be different from the IR brightness distribution. The radio emission may peak inside the IR-NE shell and have some extended emission toward the southwest.

The yellow contours in Fig. 2 are the 0.5–2.0 keV *ROSAT* High-Resolution Imager (HRI) data provided by *SkyView* and show that X-rays are distributed across the central part of the remnant along the southeast-northwest direction (see also Fig. 3 of Hughes et al. 1994).

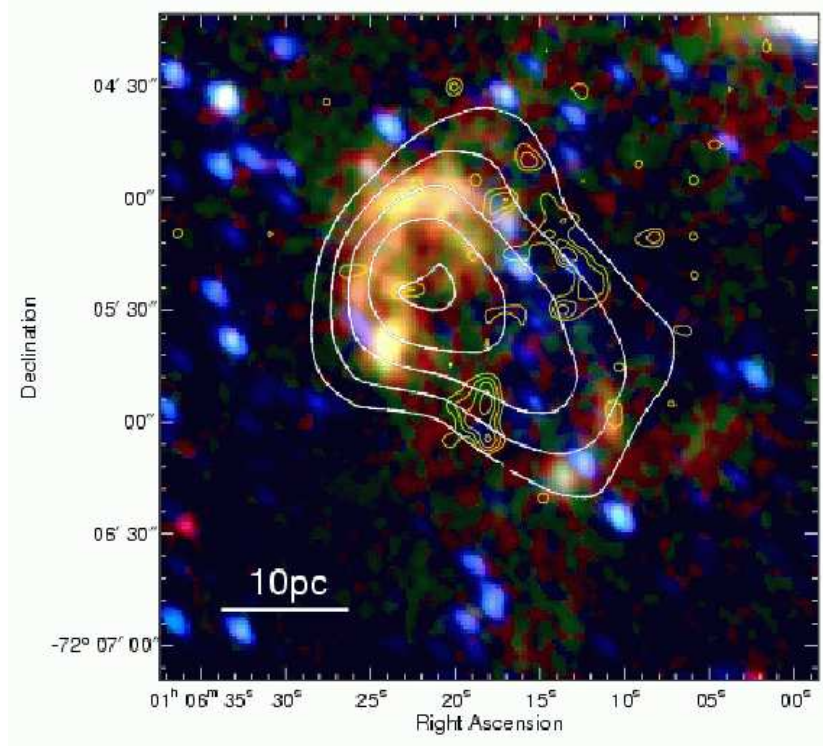


**Fig. 2.** *AKARI* three-color image generated from N4 (B), S7 (G), and S11 (R). White contours show the 843 MHz radio map of Mathewson et al. (1984) while yellow contours show the *ROSAT* HRI 0.5–2.0 keV map.

There is no apparent X-ray emission associated with the IR shell. Toward the northwest, the X-ray emission extends beyond the boundary connecting the IR NE and SW shells. The bright, compact X-ray source near the southeastern boundary of the remnant is the source identified as a Be/X-ray binary system by Hughes et al. (1994). van der Heyden et al. (2004) showed that the X-ray spectrum of the diffuse emission can be fitted by a thermal plasma model at 0.6 keV.

In the optical, B0104–72.3 has a complex morphology (Mathewson et al. 1984). We can see optical filaments coincident with the IR shells in the  $H\alpha$  and  $[S\ II] \lambda\lambda\ 6717/6731$  images of Mathewson et al. (1984). The bright spot in the IR-NE shell appears bright in the optical too, but the rest of the shell is generally faint. Instead there is brighter, filamentary optical emission all over the southwestern area and also in the northeastern area of the remnant. These optical emission features seem to correspond to the faint IR filamentary features in the N4/S7 images of Fig. 1, although the comparison is limited by the resolution and sensitivity. (We can also identify some corresponding filaments in their  $[O\ III] \lambda\ 5007$  image but only tentatively due to poor S/N ratio of the image.) In short, the IR shells have associated optical emission but this emission is faint. Instead there are bright optical filaments associated with faint IR features.

#### 4. IRC Colors and the Origin of IR Emission

In this section, we derive IRC colors of the IR shells and explore the origin of the IR emission. We derive the IRC fluxes of the shells by summing all signals inside an ellipse surrounding each of them. Point sources are excluded by putting masks on them. The same areas are masked out in all bands even if they are visible only in the NIR bands. The background contribution is estimated from surrounding annulus and is subtracted. The contamination due to the muxbleed in the bands N3 and N4 is also estimated and subtracted. The conversion to astronomical fluxes is performed by using the conversion factors in the IRC Data Users Manual, which were derived from standard stars. The fluxes are not extinction-corrected because the extinction is small. van der Heyden et al. (2004) obtained an H nuclei column density of  $4.8 \pm 1.7 \times 10^{21} \text{ cm}^{-2}$  toward the source, while the Galactic hydrogen column density toward the SMC is  $6.1 \times 10^{20} \text{ cm}^{-2}$  according to the Galactic neutral hydrogen calculator COLDEN from Chandra X-ray center. This will give an extinction of 0.04 mag at  $3.2 \mu\text{m}$  using the extinction cross sections in the Milky Way and SMC provided by Weingartner & Draine (2001)<sup>1</sup>. The results are summarized in Table 1. Table 1 shows that the IRC colors of the IR-NE shell is (N3/N4, N4/S7, S7/S11)  $\sim$  (0.7, 0.4, 0.8). For comparison, we have derived the fluxes of the bright spot in the IR-NE shell and they are listed in Table 1 too. Its IRC colors agree well with those of the IR-NE shell.

The fluxes in Table 1 are the fluxes within ellipses excluding the areas occupied by point sources, which amount to a significant portion (15–35%) of the ellipses, so that they represent rough estimates for the fluxes of the sources. The colors, however, should be relatively accurate because they are the ratios of fluxes of the same areas. The errors are due to uncertainties in the flux calibration and background subtraction. The absolute flux calibration of the IRC array for a point source is accurate to 5–6% (Onaka et al. 2007). The flux calibration for an extended source is different from a point source, because the incident lights are scattered in the IRC array and this diffuse scattered light is not included in the point source flux calibration but is partly included for an extended source (e.g., Cohen et al. 2007). According to Sakon et al. (2007), 4–5% of the incident light of a bright source is lost as scattered light spread in horizontal direction in S7 and S11. But the correction factor depends on the brightness distribution of the source and wavelength, and has not been fully studied yet. For the IR shells, which are not truly extended sources, we consider that 10% is a reasonable number for the error in color associated with this extended-source correction. Then, including the uncertainties in the background subtraction, we estimate that the uncertainties in the colors in Table 1 are  $\lesssim 15\%$  for the bright spot and  $\lesssim 30\%$  for the IR shells.

The NIR/MIR emission of SNRs could be generally composed of ionic forbidden lines, rotational and ro-vibrational lines of H<sub>2</sub> molecule, PAH (polycyclic aromatic hydrocarbon)

---

<sup>1</sup> Data available at <http://www.astro.princeton.edu/~draine/dust/dustmix.html>.

**Table 1.** IRC Fluxes and Colors of the SNR B0104–72.3.

	Area <sup>a</sup>	Flux				Color		
		N3	N4	S7	S11	N3/N4	N4/S7	S7/S11
IR-NE shell	84'' × 66''	2.4	3.2	7.8	9.5	0.75	0.41	0.82
Bright spot <sup>b</sup>	30'' × 30''	0.34	0.49	1.2	1.4	0.68	0.42	0.87
IR-SW shell	43'' × 27''	0.31	0.41	0.78	0.84	0.75	0.53	0.93
RCW 103 (Fast <i>J</i> shock) <sup>c</sup>	...	...	...	...	...	0.01	0.30	0.65
IC 443 (Molecular shock) <sup>d</sup>	...	...	...	...	...	1.1	0.44	1.1

Note. — Fluxes are the values (in mJy) at reference wavelengths when  $F_\nu \propto \nu^{-1}$ . The reference wavelengths for the N3, N4, S7, and S11 bands are 3.2, 4.1, 7.0, and 11.0  $\mu\text{m}$ . The fluxes are rough estimates of the total fluxes of the sources. The uncertainties in the colors are  $\lesssim 15\%$  for the bright spot while it is 30% for the IR shells (see text for details). For comparison, the expected IRC colors of the Galactic SNRs RCW 103 and IC 443 are listed.

<sup>a</sup> Major and minor axes of elliptical areas used for the flux calculation. The areas occupied by point sources are excluded, which amounts to 15%, 35%, and 28% for the IR-NE shell, Bright spot, and IR-SW shell.

<sup>b</sup> The bright spot in the IR-NE shell at (01<sup>h</sup> 06<sup>m</sup> 24.<sup>s</sup>1,  $-72^\circ 05' 39''$ ).

<sup>c</sup> Calculated IRC colors of a bright optical filament in RCW 103 based on the ISO spectrum of Oliva et al. (1999).

<sup>d</sup> Calculated IRC colors of shocked molecular gas in IC 443 based on the two temperature model of Rho et al. (2001). (See text for details.)

bands, or continuum emission from hot dust (e.g., see Reach et al. 2006). Synchrotron emission is usually negligible except for young Crab-like SNRs. In B0104–72.3, the radio continuum is faint and the IR brightness distribution is considered to be different from that of radio continuum (§ 3), so that the synchrotron emission contribution should be negligible. The absence of an associated X-ray emission indicates that it is probably not the thermal emission from collisionally-heated dust in X-ray emitting hot plasma. Also, the “flat” IRC color cannot be achieved unless the plasma density is unacceptably high for usual grain size distribution (see Draine 1981; Dwek 1986; Dwek, Foster, & Olaf 1996). The abundance of PAH molecules may be enhanced in SNR shells because shocks can convert a significant fraction of mass in large grains into small grains or PAHs (Jones, Tielens, & Hollenbach 1996). But the strong PAH bands are at 3.3, 6.2, 7.7, 8.6, and 11.3  $\mu\text{m}$ , so that we expect the IRC N4 band much fainter than the other bands. The IRC color of B0104–72.3 is not consistent with the PAH emission. We therefore consider that the observed NIR/MIR emission from B0104–72.3 is either forbidden ionic lines or H<sub>2</sub> lines, or both, from shock-heated gas.

The existence of the optical filaments associated with the IR shells indicates that the IR emission could be at least partly forbidden ionic lines and/or H recombination lines from fast, ionizing *J*-type shocks (hereafter fast *J* shocks; see McKee et al. 1984 for classification of

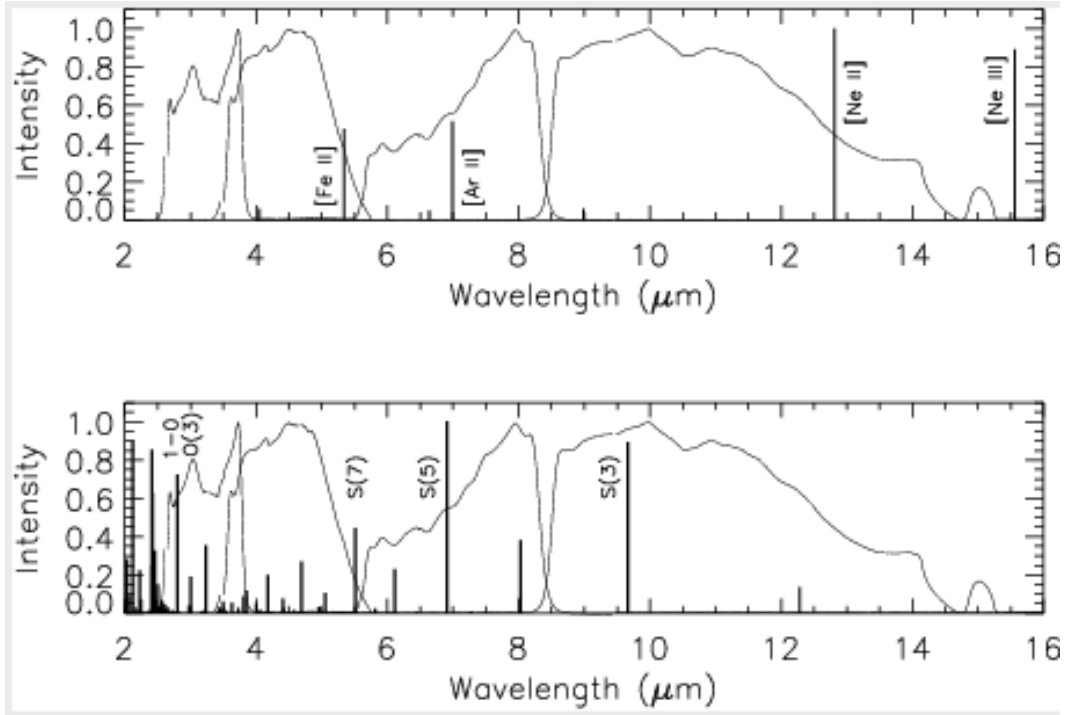
interstellar shocks) because there are optical filaments associated with the IR shells. Fig. 3 (top) shows an example of IR spectra from fast  $J$  shocks dominated by ionic lines where we overlay the spectral throughput of four IRC bands. It is an ISO spectrum toward a bright optical filament in the Galactic SNR RCW 103. The strongest lines are [Fe II] 5.34  $\mu\text{m}$  (N4), [Ar II] 6.99  $\mu\text{m}$  (S7), [Ne II] 12.81  $\mu\text{m}$  (S11), and [Ne III] 15.56  $\mu\text{m}$ . These are also generally the strongest ionic lines in this NIR/MIR band (2.0–17.0  $\mu\text{m}$ ) in other SNRs (Douvion et al. 2001a; Douvion, Lagage, & Pantin 2001b; Williams, Chu, & Guendl 2006). In the band N4, Br $\alpha$  4.05  $\mu\text{m}$  line can be as strong as or even stronger than [Fe II] 5.34  $\mu\text{m}$  line in principle (e.g., Hollenbach & McKee 1989). But previous NIR observations showed that the ratio of Br $\gamma$  2.166  $\mu\text{m}$  to [Fe II] 1.644  $\mu\text{m}$  line is usually much less ( $\sim 1/50$ ) than theoretical expectations in SNR shocks (Graham, Wright, & Longmore 1987; Oliva, Moorwood, & Danziger 1989; Koo et al. 2007), which suggests that the ratio of Br $\alpha$  to [Fe II] 5.34  $\mu\text{m}$  line might be much less than the theoretical expectation too. Note that there are no strong lines in the N3 band (2.6 to 3.8  $\mu\text{m}$ ). Hydrogen Pf series ( $n = 8-11 \rightarrow 5$ ) fall in this band, but the total intensity would be  $\sim 30\%$  of Br $\alpha$  line based on the result on Case B nebula (Hummer & Storey 1987). Therefore, if the emission is dominated by ionic lines, then the flux in N3 should be much weaker than the other three bands. The IRC colors of RCW 103, for example, would be (N3/N4, N4/S7, S7/S11)=(0.01,0.30,0.65) (Table 1). The observed IRC colors of the IR shells are not consistent with a fast  $J$  shock dominated by ionic lines and require H<sub>2</sub> molecular lines.

Fig. 3 (bottom) shows a sample spectrum from shocked molecular gas dominated by H<sub>2</sub> lines. It is a synthesized spectrum of IC 443 which is a prototypical SNR interacting with molecular clouds. The spectrum is based on the empirical, two-temperature model of Rho et al. (2001) who showed that the observed NIR/MIR spectrum of IC 443 (Richter, Graham, & Wright 1995; Cesarsky et al. 1999) can be fitted well by two components; one at  $T_{\text{ex}} = 870$  K with H<sub>2</sub> column density of  $1.3 \times 10^{21} \text{ cm}^{-2}$  and the other at  $T_{\text{ex}} = 2970$  K with  $4.0 \times 10^{18} \text{ cm}^{-2}$ . The spectrum is dominated by ro-vibrational lines in N3, and by pure rotational lines in N4, S7, and S11. The expected IRC colors of IC 443 are (N3/N4, N4/S7, S7/S11)=(1.1,0.44,1.1) (Table 1), which are not very different from those of B0104–72.3. One might be able to fit the observed color of B0104–72.3 by a shock model where the shock is slow ( $\lesssim 40\text{--}50 \text{ km s}^{-1}$ ) and molecules are not or partially dissociated as in IC 443 (e.g., Richter, Graham, & Wright 1995; Cesarsky et al. 1999). Such numerical studies, however, is beyond the scope of this paper. We simply conclude that the observed IR emission is consistent with a molecular shock, i.e., a shock propagating into molecular gas, although we cannot rule out some possible contribution from ionic lines.

## 5. Discussion

The *AKARI* result shows that B0104–72.3 has a SNR shell bright in IR. According to our analysis, the IR emission is probably from shocked molecular gas, which indicates that





**Fig. 3.** (top) An ISO spectrum toward a bright optical filament of RCW 103 (Oliva et al. 1999). The throughput of the four IRC bands, N3, N4, S7, and S11 from left to right, are overlaid. (bottom) A synthesized spectrum of molecular shock in IC 443 (see text for an explanation).

B0104–72.3 is interacting with molecular clouds (MCs). The centrally-filled thermal X-rays support this conclusion because many of the Galactic SNRs interacting with MCs do show such X-ray characteristics, e.g., Rho & Petre (1998), Koo (2003). The faint optical filaments associated with the IR shells are not unexpected, because molecular clouds are clumpy and shocks propagating through diffuse interclump medium could be fast  $J$  shocks. Most of the observed IR emission, however, might be from slow ( $\lesssim 40 \text{ km s}^{-1}$ ) non-dissociative, or partially dissociative shocks propagating into dense clumps. Such multiple shocks of different natures are expected and have been observed in several Galactic SNRs interacting with molecular clouds (e.g., Chevalier 1999, Reach & Rho 2000, Snell et al. 2005 and references therein). A prototypical one is IC 443 (G189.1+3.0; Lee et al. 2007). IC 443 is interacting with both atomic and molecular gas, so that, in the optical, its northeastern shell that is interacting with diffuse atomic gas is bright, while, in the MIR, e.g., in the Midcourse Space Experiment (MSX)  $8.28 \mu\text{m}$  band, the southern shell interacting with molecular gas is bright. Its extent (20 pc) is somewhat smaller than B0104–72.3. It also has faint optical filaments over the entire remnant. X-rays are bright inside the remnant, which is of thermal origin ( $\sim 1 \text{ keV}$ ; Kawasaki et al. 2002). Therefore, B0104–72.3 is quite similar to IC 443 and might be a middle-aged ( $\gtrsim 10^4 \text{ yrs}$ ) SNR expanding in a multiphase interstellar medium.

The interaction with MCs suggests that B0104–72.3 is possibly a core-collapse SNR

with a massive progenitor star. Our analysis indicates that the radio nebula is probably inside the IR shell, and it could be a pulsar wind nebula (PWN) considering its flat spectrum. The radio nebula appears too large for a middle-aged PWN, but it is possible that the nebula can be rejuvenated through the interaction with the SNR shell as in the Galactic SNR CTB 80 (Fesen, Shull, & Saken 1988; Koo et al. 1990). CTB 80 is another SNR where the SNR shell is detected in IR, i.e., in an IRAS 60 to 100  $\mu\text{m}$  color map. It is an old ( $\sim 1 \times 10^5$  yr) SNR where apparently its pulsar is interacting with the SNR shell to produce a large ( $\sim 40$  pc) synchrotron nebula. The flux of B0104–72.3 ( $\sim 13$  mJy at 1 GHz) is an order of magnitude less than that of CTB 80, which would be  $\sim 130$  mJy if it were in the SMC.

On the other hand, there have been suggestions that B0104–72.3 is a Type Ia SNR (Hughes et al. 1994; van der Heyden et al. 2004). It is not impossible for a Type Ia SNR to be interacting with MCs, e.g., Tycho (Lee et al. 2004). The radio nebula may have a morphology similar to the optical image rather than the IR image as in IC 443, although its spectral index is rather unusual for a shell-type SNR. A multiwavelength study with high-resolution radio observations is needed to resolve the issue.

## 6. Conclusion

B0104–72.3 is the first SNR detected in the 2.6–15  $\mu\text{m}$  bands in the SMC. It is the faintest known SMC SNR in the radio and is not particularly bright in X-rays. The brightest two SMC SNRs in X-rays are SNRs B0102–72.3 (IKT 22) and B0103–72.6 (IKT 23), which are both young oxygen-rich SNRs (van der Heyden et al. 2004). B0102–72.3 is also one of the brightest radio SNRs. B0102–72.3 was observed by Stanimirović et al. (2005) using the *Spitzer Space Telescope* and was detected at 24  $\mu\text{m}$  (80 mJy), but neither at 8 nor 70  $\mu\text{m}$ , which was interpreted as thermal emission from hot dust at  $\sim 120$  K. The  $1\sigma$  upper limit at 8  $\mu\text{m}$  was 3 mJy. B0103–72.6 was observed by us using *AKARI* (see § 2), but no NIR/MIR emission associated with the SNR shell was detected. The discovery of B0104–72.3 shows that IR bright SNRs are not necessarily radio or X-ray bright ones, or vice versa.

B0104–72.3 is bright in the IR probably because it is interacting with MCs. If B0104–72.3 were in our Galaxy, say at a distance of 1.5 kpc, its flux would be  $\sim 16$  Jy in the S7/S11 bands. For comparison, the flux of IC 443, which is at the same distance, estimated from the MSX data is  $\sim 50$  Jy at 8.28  $\mu\text{m}$ . Therefore, B0104–72.3 would be a bright, but not an exceptionally bright SNR in the Galaxy. It is also significantly fainter than the brightest NIR/MIR SNRs in the Large Magellanic Cloud, e.g., N49 and N63A, whose fluxes are 32–41 mJy and 130–300 mJy in the *Spitzer* IRAC 3.6/4.5 and 5.8/8.0  $\mu\text{m}$  bands, respectively (Williams, Chu, & Guendl 2006). N49 is also known to be interacting with MCs (Banas et al. 1997). Whether or not B0104–72.3 is the brightest NIR/MIR SNR in the SMC needs to be answered.

Our work shows that the *AKARI* IRC colors can be used for shock diagnosis. In par-

ticular, the brightness of N3 relative to the other bands is a good indicator that distinguishes between ionic and molecular shocks. A careful analysis of IRC colors might enable us to constrain the shock parameters.

We would like to thank all the members of the *AKARI* project for their dedicated work. *AKARI* is a JAXA project with the participation of ESA. This work was supported by the Korea Research Foundation (grant No. R14-2002-058-01003-0).

## References

- Banas, K. R., Hughes, J. P., Bronfman, L., & Nyman, L.-Å 1997, *ApJ*, 480, 607
- Cesarsky, D., Cox, P., Pineau des Forets, G., van Dishock, E. F., Boulanger, F., & Wright, C. M. 1999, *A&A*, 348, 945
- Cohen, M. et al. 2007, *MNRAS*, 374, 979
- Chevalier, R. A. 1999, *ApJ*, 511, 798
- Draine, B. T. 1981, *ApJ*, 245, 880
- Douvion, T., Lagage, P. O., Cesarsky, C. J., Dwek, E. 2001, *A&A*, 373, 28
- Douvion, T., Lagage, P. O., Pantin, E. 2001, *A&A*, 369, 589
- Dwek, E. 1986, *ApJ*, 302, 363
- Dwek, E., Foster, S. M., & Olaf, V. 1996, *ApJ*, 457, 244
- Fesen, R. A., Shull, J. M., Saken, J. M. 1988, *Nature*, 334, 229
- Filipović, M. D., Payne, J. L., Reid, W., Danforth, C. W., Staveley-Smith, L., Jones, P. A., White, G. L. 2005, *MNRAS*, 364, 217
- Graham, J. R., Wright, G. S., & Longmore, A. J. 1987, *ApJ*, 313, 847
- Hollenbach, D. & McKee, C. F. 1989, *ApJ*, 342, 306
- Hughes, J. P., Smith, R. C. 1994, *AJ*, 107, 1363
- Hummer, D. G. & Storey, P. J. 1987, *MNRAS*, 224, 801
- Ita, Y. & Peason, C. 2007, *IRC Imaging Data Reduction Pipeline User Manual*
- Jones, A. P., Tielens, A. G. G. M., & Hollenbach, D. J. 1996, *ApJ*, 469, 740
- Kawasaki, M., Ozaki, M., Nagase, F., Masai, K., Ishida, M., & Petre, R. 2002, *ApJ*, 572, 897
- Koo, B.-C. 2003, in *The Proceedings of the IAU 8th Asian-Pacific Regional Meeting (ASP Conference Proceedings v. 289)*, ed Ikeuchi, S., Hearnshaw, J. & Hanawa, T. (San Francisco: ASP), page 199
- Koo, B.-C., Reach, W. T., Heiles, C., Fesen, R. A., & Shull, J. M. 1990, *ApJ*, 364, 178
- Koo, B.-C., Moon, D.-S., Lee, H.-G., Lee, J.-J., & Mathews, K. 2007, *ApJ*, 657, 308
- Lee, J.-J., Koo, B.-C., & Tatematsu, K. 2004, *ApJL*, 605, 113
- Lee, J.-J., Koo, B.-C., Yun, M. S., Stanimirović, S., Heiles, C., Heyer, M. 2007, *AJ*, submitted
- Mathewson, D. S., Ford, V. L., Dopita, M. A., Tuohy, I. R., Mills, B. Y., Turtle, A. J. 1984, *ApJS*, 55, 189
- McKee, C. F., Chernoff, D. F., & Hollenbach, D. J. 1984, in *Galactic and Extragalactic Infrared Spectroscopy*, ed. Kessler, M. F. & Phillips, J. P. (Dordrecht: D. Reidel), page 103
- Oliva, E., Moorwood, A. F. M., & Danziger, I. J. 1989, *A&A*, 214, 307
- Oliva, E., Moorwood, A. F. M., Drapatz, S., Lutz, D., & Sturm, E. 1999, *A&A*, 343, 943

Onaka, T. et al. 2007, in this volume  
Park, S., Hughes, J. P., Burrows, D. N., Slane, P. O., Nousek, J. A., & Garmire, G. P. 2003, ApJL, 598, L95  
Reach, W. T., & Rho, J. 2000, ApJ, 544, 843  
Reach, W. T. et al. 2006, AJ, 131, 1479  
Rho, J. & Petre, R. 1998, ApJL, 503, L167  
Rho, J., Jarrett, T. H., Cutri, R. M., & Reach, W. T. 2001, ApJ, 547, 885  
Richter, M. J., Graham, J. R., & Wright, G. S. 1995, ApJ, 454, 277  
Sakon, I. et al. 2007, in this volume  
Snell, R. L., Hollenbach, D., Howe, J. E., Neufeld, D. A., Kaufman, M. J., Melnick, G. J., Bergin, E. A., & Wang, Z. 2005, ApJ, 620, 758  
Staminirovic, S., Bolatto, A. D., Sandstrom, K., Leroy, A. K., Simon, J. D., Gaensler, B. M., Shah, R. Y., Jackson, J. M. 2005, ApJ, 632, L103  
van der Heyden, K. J., Bleeker, J. A. M., Kaastra, J. S. 2004, A&A, 421, 1031  
Weingartner, J.C. & Draine, B.T. 2001, ApJ, 548, 296  
Williams, R. M., Chu, Y.-H., & Gruendl, R. 2006, ApJ, 132,1877